Extended characterisation of ITER strands - (MS-MG) TARSIS Action No F4E-2009-GRT-029. Samples 1, 2 and 3 (of 6)

Yeekin Tsui, Mark Raine and Damian Hampshire

Fusion Energy Reference Laboratory -

Metrology of Superconducting Strands.

Superconductivity Group, Centre for Materials Physics,

Physics Department, Durham University,

Durham DH1 3LE, UK.

1. Document Reference	Extended characterisation of ITER strands Tarsis samples 1,2 and 3 (of 6)	Revision:	2
2. F4E Reference	Action: F4E-2009-GRT-029	2.1 F4E TRO	D. Hampshire
3. F4E Customer Reference	Durham University		
4. SUPPLIER	Durham University		
5. Order Title	Extended characterisation of ITER strands (MS-MG) TARSIS Action No F4E-2009-GRT-029		
6. Graded Quality Level	CLASS 2		
7. Date for current revision	1st Feb 2012		

Revisions Table		
Revision Number	**Revision Details**	**Date**
2	Comparison removed	01/02/2012
1	RMS Error bars corrected + comparison with the literature (post Barcelona meeting) added.	04/09/2011
0	Original document – no revisions	06/07/2011

TABLE OF CONTENTS

ACKNOWLEDGEMENTS

The authors acknowledge the help and support of Thierry Boutboul (F4E), Peter Readman (F4E) and Arend Nijhuis (Twente U.).
We also acknowledge the many discussions we have had with those in the F4E and ITER community including: Neil Mitchell and Armand Nyilas.

IPR STATEMENT

The important results from the task are summarised in the abstract and described in detail in the accompanying report – there was no IPR created in the course of this work.
Pre-existing knowledge is outlined in the publicly available literature – in particular the published reports and articles of those scientists cited in the reference section of this report.
There is no foreground IPR – all techniques used are encompassed within the publicly available state-of-the-art literature.
There is no new business confidential information, business confidential know-how, or trade secrets - the materials used in this report were supplied without any obligations re confidentiality.
Disclosure of the information – this report will be made available through the public-accessible Web in the first instance and thereafter discussed at specialist scientific meetings and published in international scientific journals.

Prof. Damian P. Hampshire Durham University
July 6th 2011.

ABSTRACT

Comprehensive measurements are reported of the engineering critical current density ($J_C(B,T,\varepsilon)$) at 10 μVm^{-1} and $n(B,T,\varepsilon)$ over the range 10 – 100 μVm^{-1} as a function of magnetic field, temperature and uniaxial strain for three different strands: an OST internal-tin Nb_3Sn strand (Billet 10536); two BEAS bronze-route Nb_3Sn strands (BEAS I and BEAS II) which are nominally the same wire (Sample 01BR8305A01C) but were given different heat-treatments - the classic ITER heat-treatment finishing with 100 hrs. at 650 C and a 2nd heat-treatment finishing with 320 hrs at 620 C (cf. table I below).

The three strands are parameterised using the Durham scaling law and the ITER scaling law both of which have nine free-parameters – the RMS values show that the $J_C(B,T,\varepsilon)$ data is most accurately described using the Durham Scaling law. The relationship between the *n*-value and critical current (I_C) is parameterised using a modified power law of the form $n = 1+rI_C^s$, where *r* and *s* are constants.

We have found:

- At 4.2 K, 12 T and zero intrinsic strain, the OST strand has the highest J_C (~ 40% higher than BEAS samples) and the J_C of BEASI strand is ~ 3% higher than that of BEASII (cf. figure 1(a)).
- For these 3 samples there are systematic trends. The higher J_C is associated with higher intrinsic parameters $T_C^*(0)$ and $B_{C2}^*(0,0)$ and higher $|c_2|$ and $|c_3|$. This leads to greater strain sensitivity for the current density of the higher J_C samples.
- We have indentified a pivot point in compressive strain which increases with increasing field and temperature. Changing the strain from one side of the pivot point side to the other, changes the highest J_C sample to the lowest J_C sample and vice versa. For the three samples measured, at 4.2K and 12 T the pivot point has a compressive strain value of -0.9 % that increases to -0.7% at 14 T.

- At 4.2 K, 12 T and zero applied strain, the OST sample has the lowest *n*-values (~ 25% lower than BEAS samples - cf. figure 1(b)).
- The *n*-values (and values of *r* and *s*) are similar for the two BEAS samples.
- The normalised strain dependence of *n* is similar for all three strands.

Accompanying this report are three spreadsheets that contain tabulations of the J_C and *n*-value data, as well as the scaling-law parameterisation of $J_C(B,T,\varepsilon)$ for OST, BEASI and BEASII strands respectively at: http://www.dur.ac.uk/superconductivity.durham/publications.html

1 INTRODUCTION

The effect of strain on Nb_3Sn strands is very important[1] because large strains are unavoidable in large magnets. The strains can originate from the differential thermal contraction between the components of the magnets during the process of cool-down and also from the large Lorentz forces produced during high-field operation. The J_C versus strain-dependence of Nb_3Sn strands has a significant impact on the design and final performance of large Cable-in-Conduit Conductors (CICC) like those used in ITER. For several years the Summers Scaling Law was widely accepted and used to describe J_C of Nb_3Sn strands. However, measurements on the Model Coil and (more recently on) advanced strands showed significant deviations from the functional form given by Summers, especially at high compressive strain. It has long been known that the strand layout and composition (ternary or quaternary compounds with Ta and/or Ti additions) influences the magnitude, field and temperature dependence of the critical current. It is now clear that for any conductor design, it is necessary to know J_C as a function of field, temperature and strain, if one wants to ensure accurate reliable conductor performance predictions.

One facility capable of measuring the field (B) and strain (ε) dependence of the critical strand current at variable temperatures (T) is available here at the University of Durham. In the framework of the European Fusion Technology programme (F4E and EFDA), the University of Durham has been involved in several strand characterization tasks (e.g. EFDA contracts 02-662, 03-1126 and 05-1296), and has a lot of experience in sample preparation, testing and evaluation of the results[1]. The broad objectives of this current task are two-fold:

i) A comprehensive characterization of $J_C(B,T,\varepsilon)$ and n-values for an advanced internal-tin (OST) Nb_3Sn strand.

ii) A comprehensive characterization of $J_C(B,T,\varepsilon)$ and n-values for two bronze-route (BEASI and BEASII) Nb_3Sn strands. These strands are nominally the same wire but were heat-treated using different schedules.

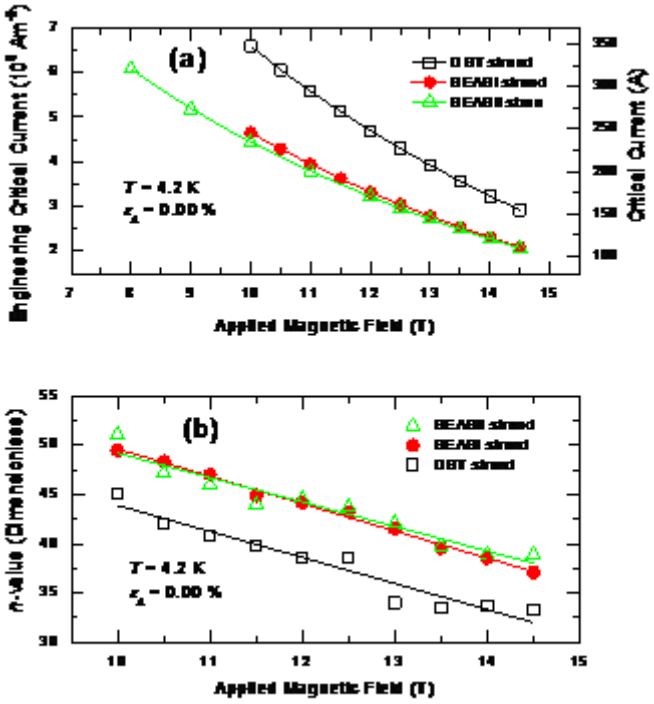

Fig. 1.(a) Engineering critical current density J_C (and critical current I_C) and (b) *n*-value versus magnetic field for Nb_3Sn strands made by different manufactures. OST is an advanced internal-tin strands. The BEASI and BEASII are bronze-route strands.

The report is structured as follows: Section 2 outlines the experimental procedure. Section 3 presents the experimental results, analysis and summary for the OST sample and the two BEAS samples. Sections 3.1 and 3.2 present the results. Section 3.3 presents the $J_C(B,T,\varepsilon)$ scaling-law parameterization and the parameterisation of the *n*-value data for the three strands using both the Durham scaling law and the official ITER scaling law proposed for characterising Nb_3Sn strands. Finally, section 4 presents the concluding comments which includes a comparison between the strands.

2 EXPERIMENTAL PROCEDURE

2.1 Sample heat-treatment

Measurements were performed on the Nb_3Sn strands using well-established procedures. All strands were heat-treated in an argon atmosphere. Table I shows the heat-treatment schedules and

the sample identification numbers for the 3 samples. The samples were all reacted on oxidised stainless-steel mandrels in a three-zone furnace, with an additional thermocouple positioned next to the sample in order to monitor the temperature. The strands were then etched in hydrochloric acid to remove the chrome plating. The strands were transferred to Cu-Be helical springs, to which they were attached by copper plating and soldering. The helical springs used for these measurements have four central turns and a rectangular cross-section [2,3].

BEAS strand I (Sample 01BR8305A01C)	OST strand (Billet 10536) BEAS strand II (Sample 01BR8305A01C)
Ramp at 5°C h^{-1} to 595°C and hold for 160 h	Ramp at 5°C h^{-1} to 210°C and hold for 50 h
Ramp at 5° C h^{-1} to 620°C and hold for 320 h	Ramp at 5° C h^{-1} to 340°C and hold for 25 h
Ramp at 5° C h^{-1} to 500°C	Ramp at 5° C h^{-1} to 450°C and hold for 25 h
Cool to room temperature inside furnace	Ramp at 5° C h^{-1} to 575°C and hold for 100 h
	Ramp at 5° C h^{-1} to 650°C and hold for 100 h
	Ramp at 5° C h^{-1} to 500°C
	Cool to room temperature inside furnace

Table I Heat-treatment schedules and sample identification numbers for the OST, BEASI and BEASII strands.

2.2 Using the Durham $J_C(B,T,\varepsilon)$ probe

The Durham strain probe[2,4] was used to carry out voltage–current (V–I) measurements on the strands as a function of magnetic field (B), temperature (T) and applied axial strain (ε_A). The spring (and sample) were mounted onto the probe and the strain was applied by twisting the spring via concentric shafts: the inner shaft connects a worm-wheel system at the top of the probe to the top of the spring, and the outer shaft is connected to the bottom of the spring via an outer can. For measurements at 4.2 K, the outer can contains a number of holes to admit liquid helium from the surrounding bath. For measurements above 4.2 K, the outer can forms a vacuum space around the sample with a copper gasket and knife edge seal between the can and the outer shaft. The temperature is controlled via three independent pairs of Cernox thermometers and constantan wire

heaters[6]. A detailed description of the experimental apparatus and techniques can be found elsewhere [2,4,5].

The measurements consist of monitoring the voltage across different sections of the sample as a function of the current through it. J_C (or I_C) was measured (is defined) at an electric field criterion of 10 μVm^{-1}.

3 RESULTS AND ANALYSIS

This report presents critical current (I_C) and engineering critical current density (J_C) data defined at an electric-field criterion of 10 μVm^{-1}, where J_C is calculated by dividing the critical current by the total cross-sectional area of the strand. OST and BEAS strands have the diameter/total cross-sectional area of 0.820 mm (manufacturers value)/5.281 × 10^{-7} m^2 and 0.808 mm (measured using SEM)/5.128 × 10^{-7} m^2 respectively. We choose to quote an engineering J_C, rather than the often used non-Cu J_C or J_C in the superconducting layer to avoid any ambiguity or loss of clarity that can occur if the nominal value for the Cu/non-Cu ratio or the area or distribution of the reacted Nb_3Sn material in the strand is subsequently found to be significantly different from the nominal values.

3.1 OST sample data

3.1.1 OST $J_C(B,T,\varepsilon)$ data

Figure 2 shows typical electric field–current density (*E-J*) (and voltage–current: *V-I*) characteristics measured at 4.2 K and ε_A = -0.30 %. The noise in these measurements is about 10 nanovolts – primarily the Johnson noise from the room-temperature section of the voltage leads. It is clear that these characteristics are not straight lines. Nevertheless for magnet engineering purposes, it is helpful to obtain *n*-values which are calculated using the power law expression $E = \alpha J^n$ for *E* between 10 and 100 μVm^{-1}.

Figure 3a is a plot of J_C (and I_C) as a function of applied strain at 4.2 K for the OST sample for magnetic fields at and below 14.5 T with field increments of 0.5 T. After the compressive measurements at 4.2 K had been completed, the sample was warmed to room temperature so the variable temperature outer can could be installed. The sample was then recooled to cryogenic temperatures and measurements made at 8 K, 10 K and 12 K. The J_C (and I_C) data as a function of applied strain at 4.2 K and 8 K are shown in figure 3. Figure 4 shows data taken at 10 K and 12 K. Figure 5 shows some reversible critical current data taken at 10 K over a range of different strains.

The data provide strong evidence that J_C is reversible under strain in these measurements and hence that the strand filaments have remained undamaged. The engineering J_C of the OST samples is the highest among the three strands as shown by the data in figure 1 taken at zero applied strain. In figures 3 and 4, the solid/dashed lines were provided by the Durham/ITER scaling law respectively and are discussed in section 3.3.

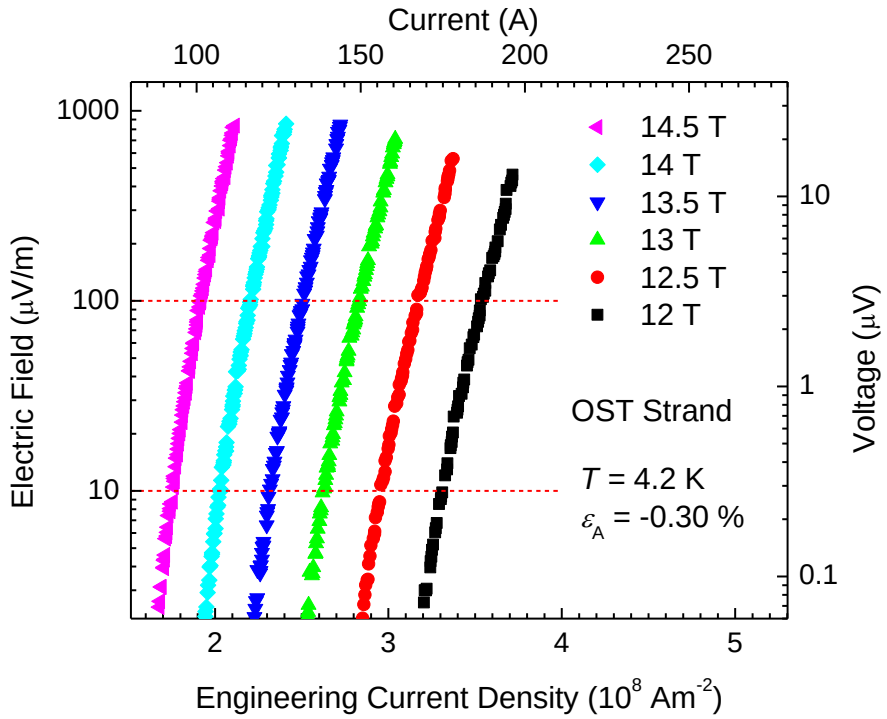

Fig. 2. Log-log plot of electric field versus current (and voltage versus current) for the OST strand at 4.2 K, with ε_A = - 0.30% in magnetic fields between 12 T and 14.5 T in increments of 0.5 T.

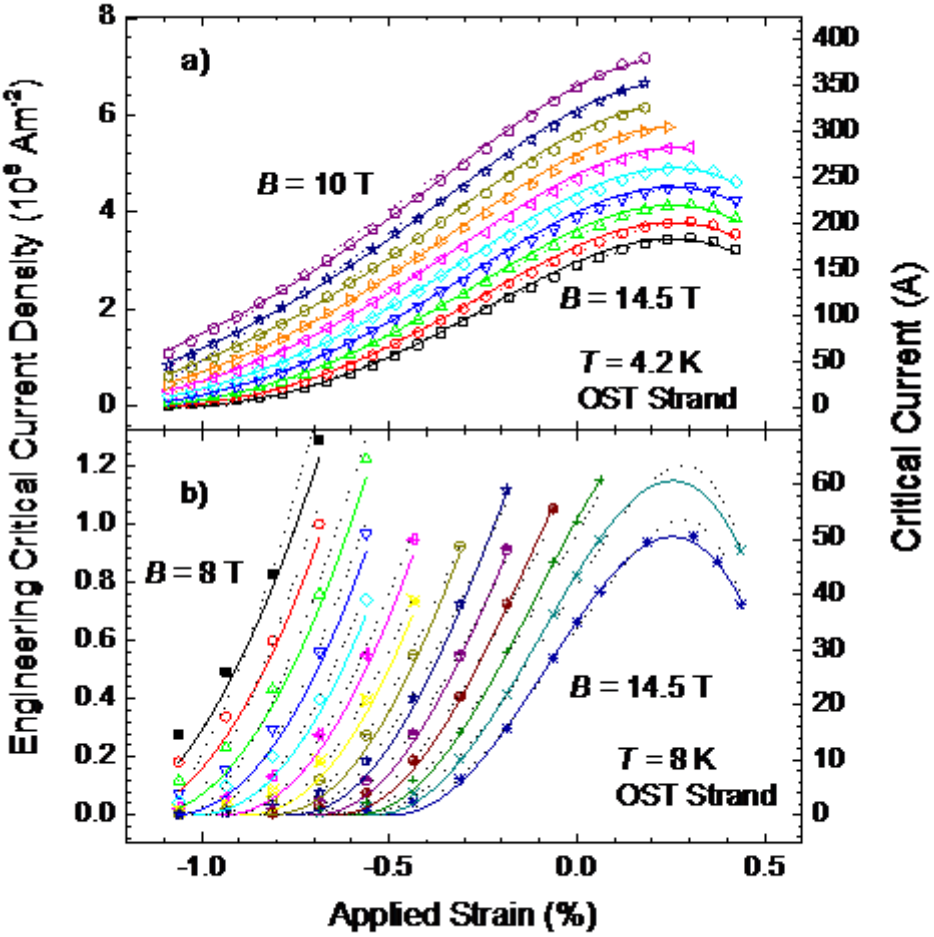

Fig. 3. Engineering critical current density (and critical current) of OST strand as a function of applied strain at (a) 4.2 K in magnetic fields from 10 to 14.5 T in increments of 0.5 T and at (b) 8 K in fields from 8 to 14.5 T in increments of 0.5 T. The solid lines are provided by the Durham scaling law[6] using the 9 free parameters listed in table II. The dotted lines are provided by the ITER scaling law[7] (parameters in table III).

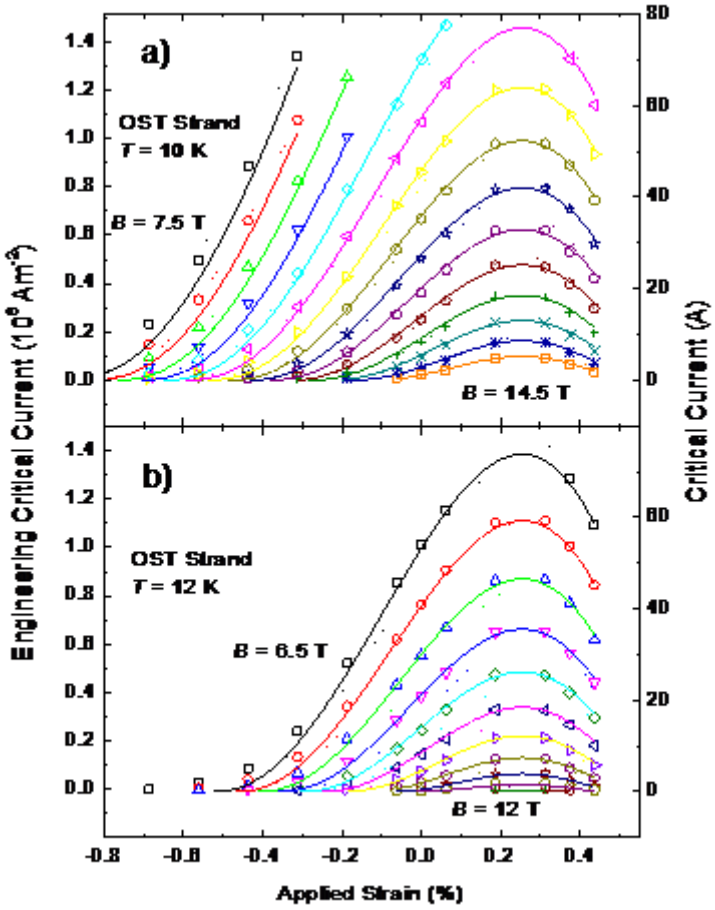

Fig. 4. Engineering critical current density (and critical current) of OST strand as a function of applied strain in magnetic fields (a) from 7.5 to 14.5 T at 10 K, and (b) from 6.5 to 12 T at 12 K. The increment of the magnetic fields is 0.5 T. The solid lines are provided from fitting the 9 free-parameter Durham scaling law. The dotted lines are provided by the ITER scaling law.

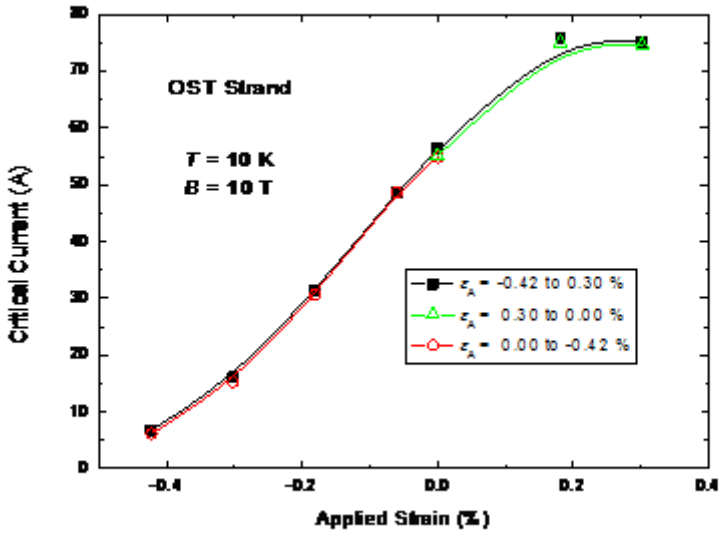

Fig. 5: The critical current as a function of applied strain at 10 T and at T = 10 K, for the OST strand. The lines are guides to the eye.

3.1.2 OST - $n(B,T,\varepsilon)$ data

Using the power-law expression $E = \alpha J^n$ and fitting the E-J data over the range from 10 to 100 μVm^{-1}, values of n were obtained. The n-values of the OST strand as a function of intrinsic strain ε_I are displayed in figure 6 where T = 4.2 K, B = 14.5 T along with the two BEAS Nb_3Sn strands. The n-values for the OST strand are smaller than the BEAS Nb_3Sn strands. It can be seen that the strain–dependence of the n-value shows a similar inverted quasi-parabolic behaviour to the critical current density. In order to parameterise the relationship between the n-value and critical current, n-1 versus critical current is plotted as shown in figure 7 and values for r and s found.

3.2 BEAS samples data

3.2.1 $J_C(B,T,\varepsilon)$ data

Figures 8 to 11 show J_C (and I_C) of the BEASI and BEASII strands as a function of applied strain at temperatures from 4.2 K to 12 K for magnetic fields at and below 14.5 T. Figures 12 and 13 show the strain reversibility of the data for the two samples taken at 4.2 K and 10 T. The data provide strong evidence that as with the OST measurements, the strand filaments have remained undamaged throughout these measurements.

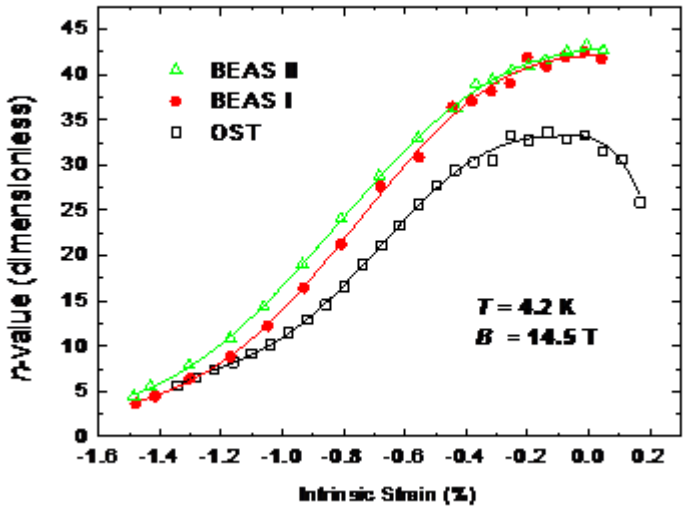

Fig. 6: *n*-value as a function of intrinsic strain for OST strand compared with other BEAS strands. Lines are guides to the eyes.

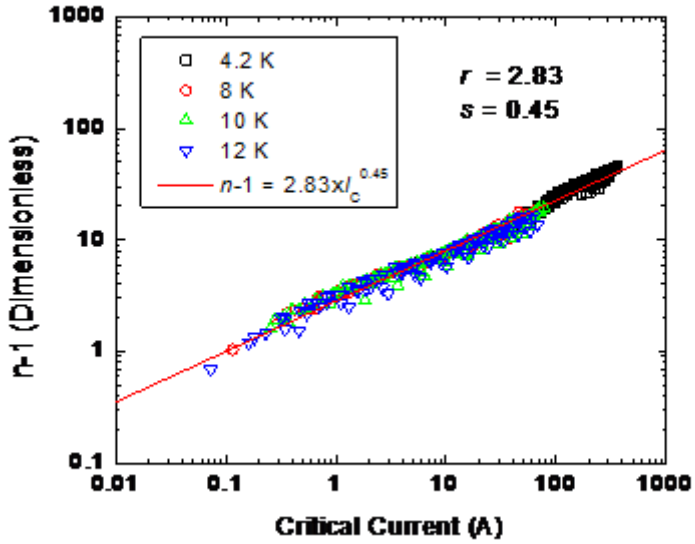

Fig. 7: The *n*-value obtained from fitting the experimental data to the equation $E = \alpha J^n$ over the range from 10 to 100 μVm^{-1}. Data are shown for the OST strand plotted as *n*-1 as a function of critical current at T = 4.2 K, 8 K, 10 K and 12 K in different fields. The line shows a fit to all the data using equation (9) where r = 2.83 and s = 0.45.

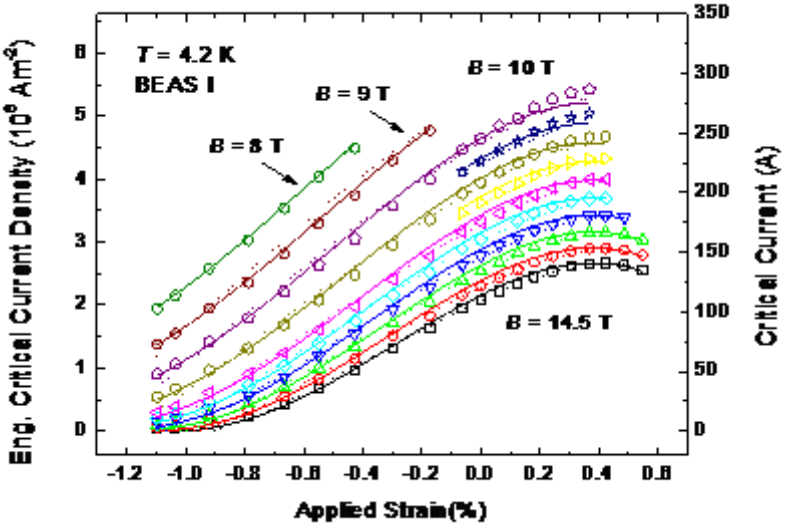

Figure 8. Engineering critical current density (and critical current) as a function of applied strain at 4.2 K and magnetic fields between 8 and 14.5 T for the BEASI strand. The solid lines are provided by the Durham scaling law[6] using 9 free parameters listed in table IV. The dotted lines are provided by the ITER scaling law[7] (parameters in table V)

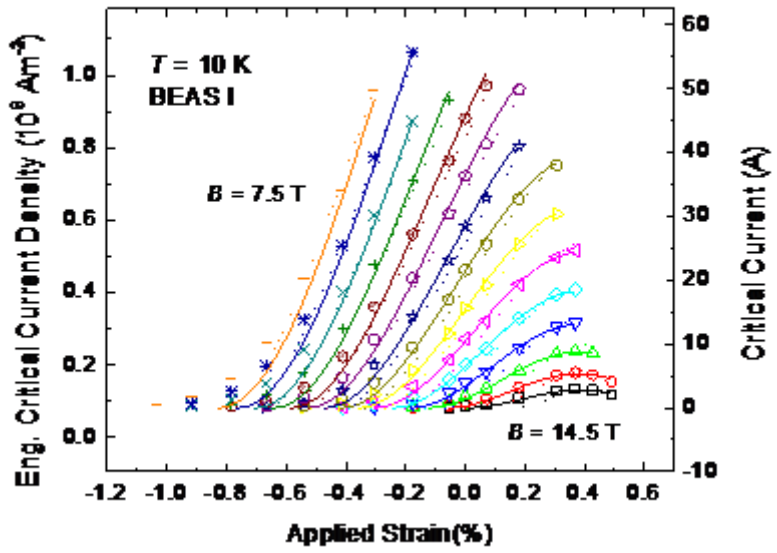

Figure 9. Engineering critical current density (and critical current) as a function of applied strain at 10 K and magnetic fields between 7.5 and 14.5 T for the BEASI strand. The solid lines are provided by the Durham scaling law[6] using 9 free parameters listed in table IV. The dotted lines are provided by the ITER scaling law[7] (parameters in table V).

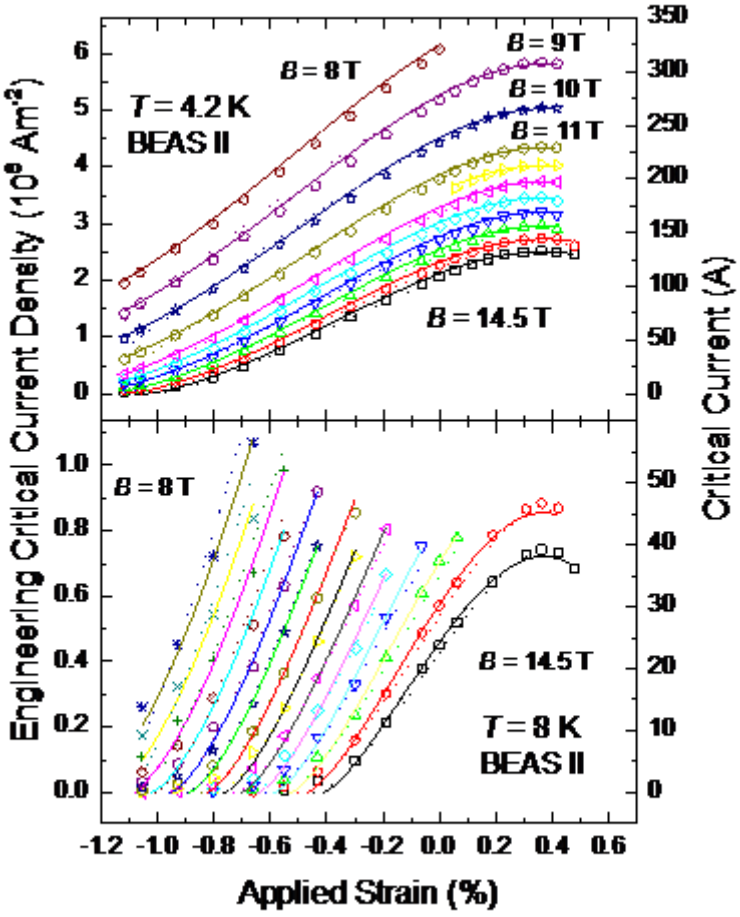

Figure 10. Engineering critical current density (and critical current) of BEASII strand as a function of applied strain at (a) 4.2 K in magnetic fields from 8 to 14.5 T and at (b) 8 K in fields from 8 to 14.5 T in increments of 0.5 T. The solid lines are provided by the Durham scaling law[6] using 9 free parameters listed in table VI. The dotted lines are provided by the ITER scaling law[7] (parameters in table VII).

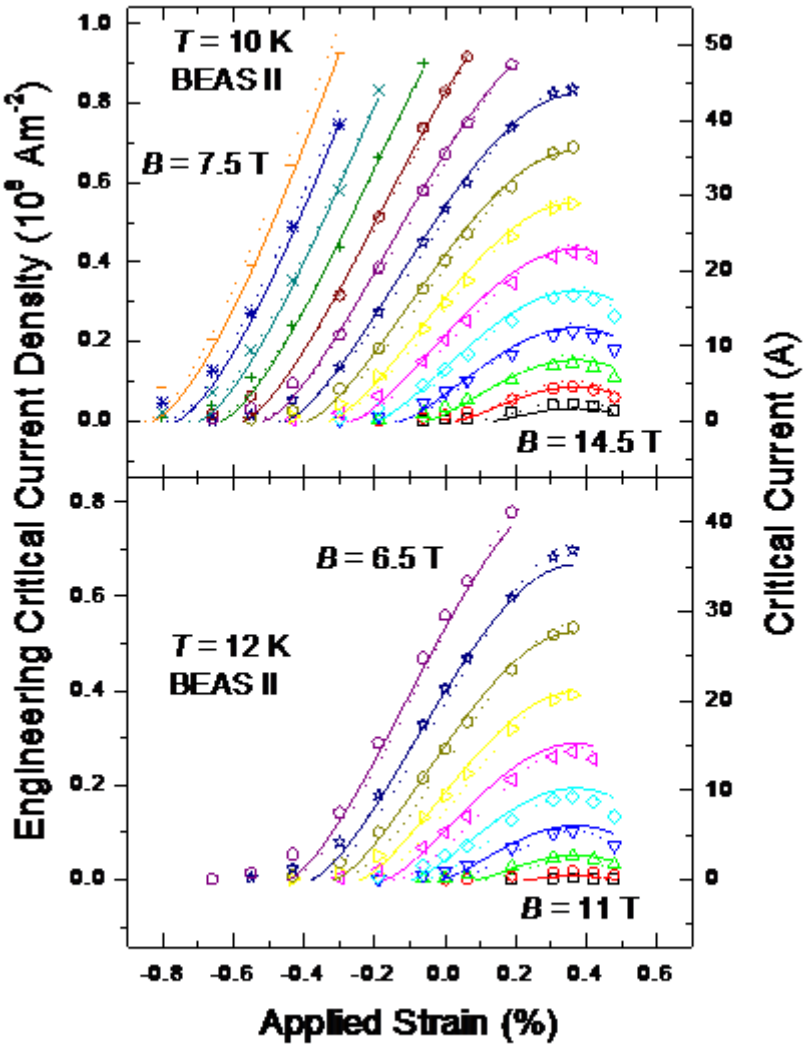

Figure 11. Engineering critical current density (and critical current) of BEASII strand as a function of applied strain at (a) 10 K in magnetic fields from 7.5 to 14.5 T in increments of 0.5 T and at (b) 12 K in fields from 6.5 to 11 T in increments of 0.5 T. The solid lines are provided by the Durham scaling law[6] using 9 free parameters listed in table VI. The dotted lines are provided by the ITER scaling law[7] (parameters in table VII).

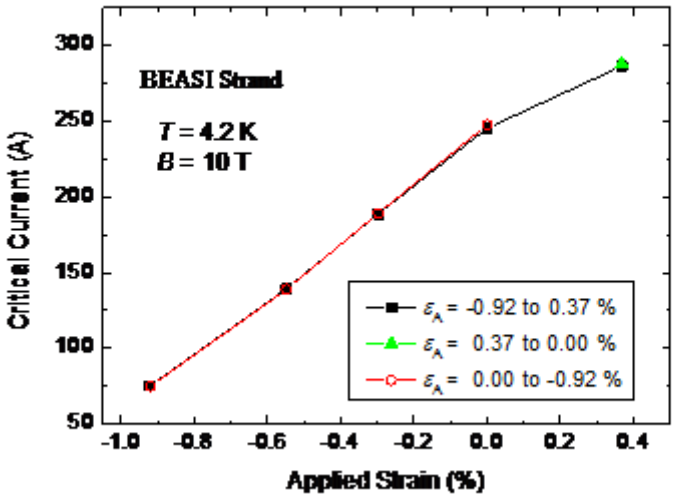

Fig. 12: The critical current as a function of applied strain at 10 T and at T = 4.2 K, for the BEASI strand. The lines are guides to the eye.

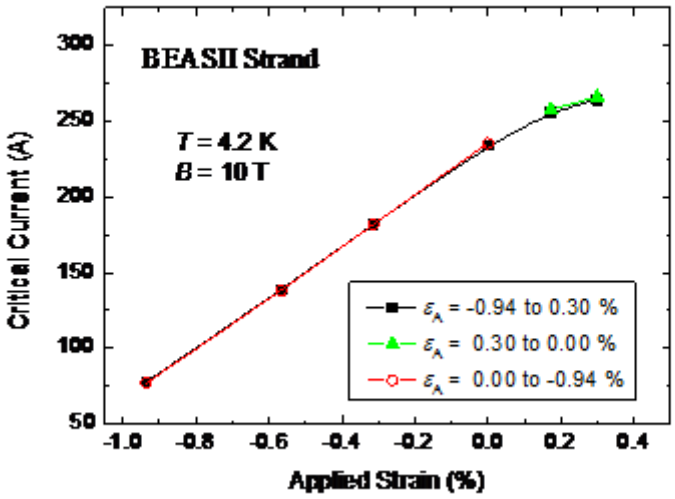

Fig. 13: The critical current as a function of applied strain at 10 T and at T = 4.2 K, for the BEASII strand. The lines are guides to the eye.

3.2.2 $n(B,T,\varepsilon)$ data

As with the OST sample, we have used the E-J data to fit the power-law expression $E = \alpha J^n$ over the range from 10 to 100 μVm^{-1}, to obtain values of n for BEASI and BEASII strands. In order to parameterise the relationship between the n-value and critical current, n-1 versus critical current is plotted as shown in figures 14 and 15. The straight lines in these figures are provided by the power laws shown. It can seen that the fitting parameters r and s are almost identical for the two BEAS strands.

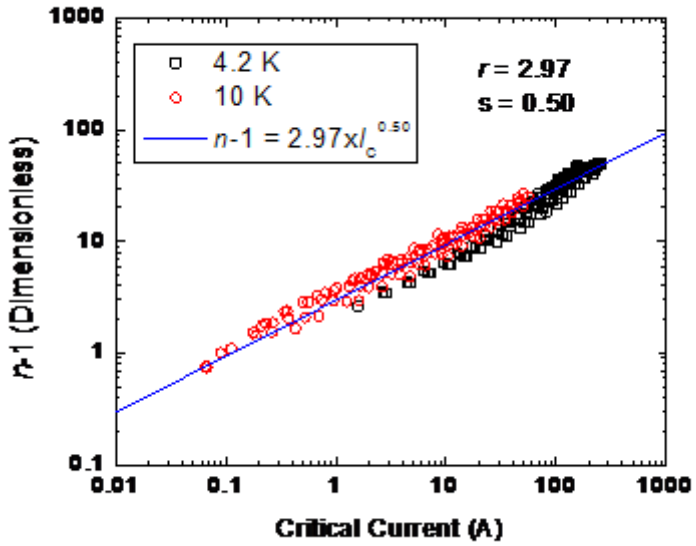

Fig. 14: The *n*-value obtained from fitting the experimental data to the equation $E = \alpha J^n$ over the range from 10 to 100 μVm^{-1}. Data are shown for the BEASI strand plotted as *n*-1 as a function of critical current at T = 4.2 K and 10 K in different fields. The line shows a fit to all the data using equation (9) where r = 2.97 and s = 0.50.

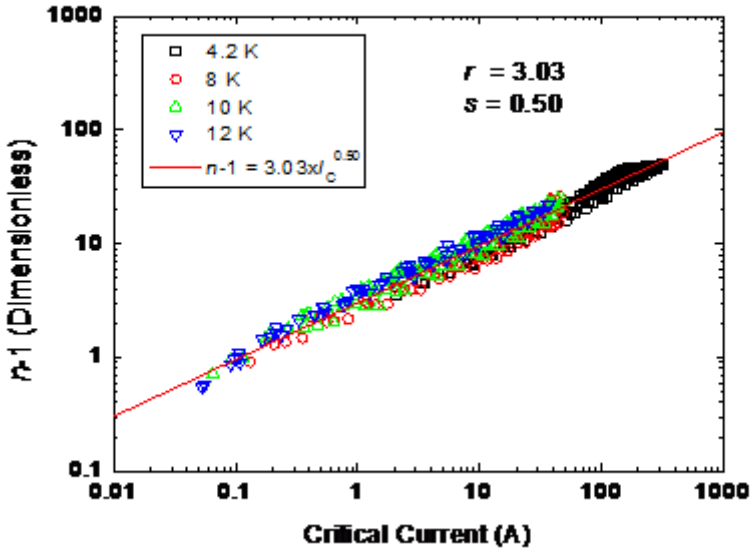

Fig. 15: The *n*-value obtained from fitting the experimental data to the equation $E = \alpha J^n$ over the range from 10 to 100 μVm^{-1}. Data are shown for the BEASII strand by plotting *n*-1 as a function of critical current at T = 4.2 K, 8 K, 10 K and 12 K in different fields. The line show a fit made using equation (9), where r = 3.03 and s = 0.50.

3.3 Critical current and *n*-value parameterisation

3.3.1 Durham and ITER scaling laws for critical current density

i) Durham Scaling Law

The $J_C(B,T,\varepsilon)$ data at 10 μVm^{-1} are parameterised using the Durham scaling law[2], which involves the following relations:

$$J_C(B,T,\varepsilon_I) = A(\varepsilon_I)\left[T_C^*(\varepsilon_I)\left(1-t^2\right)\right]^2\left[B_{C2}^*(T,\varepsilon_I)\right]^{n-3} b^{p-1}(1-b)^q \quad (1)$$

$$B_{C2}^*(T,\varepsilon_I) = B_{C2}^*(0,\varepsilon_I)\left(1-t^\nu\right) \quad (2)$$

$$\left(\frac{A(\varepsilon_I)}{A(0)}\right)^{1/u} = \left(\frac{B_{C2}^*(0,\varepsilon_I)}{B_{C2}^*(0,0)}\right)^{1/w} = \frac{T_C^*(\varepsilon_I)}{T_C^*(0)} \quad (3)$$

$$\frac{B_{C2}^*(0,\varepsilon_I)}{B_{C2}^*(0,0)} = 1 + c_2\varepsilon_I^2 + c_3\varepsilon_I^3 + c_4\varepsilon_I^4, \quad (4)$$

$$\varepsilon_I = \varepsilon_A - \varepsilon_M, \quad (5)$$

where J_C is the engineering critical current density (the critical current divided by the total cross-sectional-area of the strand), ε_A is the applied strain, ε_I is the intrinsic strain, ε_M is the applied strain at the peak, T_C^* is the effective critical temperature, $t = T/T_C^*$ is the reduced temperature, B_{C2}^* is the effective upper critical field and $b = B/B_{C2}^*$ is the reduced field.

To date we have found that if comprehensive data are available, a 13 free-parameter fit is best for engineering purposes. However in many cases, there is little loss of accuracy parameterising the strands if the number of free parameters is reduced to 9 and universal values of n = 2.5, ν = 1.5, w = 2.2, u = 0 are used[2].

ii) ITER scaling Law

The extensive data in this work has also been parameterised using a scaling law[7] proposed for characterising interlaboratory measurements of ITER strands. It has 9 free parameters and is of the form:

$$J_C(B,T,\varepsilon_I) = \frac{C}{B} s(\varepsilon_I)(1-t^{1.52})(1-t^2)b^p(1-b)^q \ . \qquad (7)$$

where $s(\varepsilon_I)$ is a specified function of strain. This equation follows work that considers the 3-dimensional nature of strain into the scaling law[8]. It effectively includes a 1/κ term[9] . This can be contrasted with the $1/\kappa^2$ found in the Durham scaling law which is consistent with experiment data[2], computational work[13] and theory[14]. The concerns about the 1/κ choice have been discussed previously [6].

3.3.2 *n*-value parameterization

The *n*-value is defined via the following relation:

$$E = \alpha J^n \qquad (8)$$

where E is the electric field and J is the (engineering) current density. A tabulation of the $J_C(B,T,\varepsilon)$ and $n(B,T,\varepsilon)$ data for OST strand and two BEAS strands can be found in the spreadsheets that accompany this report[10]. The *n*-value is commonly used as a 'quality index' for the superconducting materials[11-13,14,15]. The origin of the *n*-value in superconducting strands can be attributed to the distributions in the critical current and the flux-flow resistivity within the filaments[12-14,16-18]. In some simples cases, non-uniformity of the filaments can be the most important factor that determines the *n*-value [13,14,17,19], in others intrinsic effects are important[18]. Given the similar inverted quasi-parabolic behaviour found for both *n* and the critical current as well as the experimental result that *n* approaches to 1 as I_C to zero, the relationship between *n*-value and the critical current is parameterised using the following modified power law[25],

$$n(B,T,\varepsilon_I) = 1 + r(T,\varepsilon_I)\left[I_C(B,T,\varepsilon_I)\right]^{s(T,\varepsilon_I)}. \qquad (9)$$

The relation between *n* and the critical current is shown in figures 7, 14 and 15 where we find that both $s(T,\varepsilon_I)$ and $r(T,\varepsilon_I)$ are only very weakly dependent on the applied strain. Detailed understanding of the connectivity between the superconducting regions and the low-resistivity normal regions will be required to provide further insight into *n*-values.

3.3.3 Parameterisation of the OST strand.

The $J_C(B,T,\varepsilon)$ data sets (cf. Figures 3 and 4) for the OST Nb_3Sn strand were parameterised using scaling laws with just 9 free-parameters. The parameters from the Durham Scaling law are given in table II (the four parameters in bold are not varied in the fitting procedure). The data were also parameterized using the official ITER scaling law and the free parameters are given in table III. The RMS difference between the measured I_C and parameterized values is ~ 2.8 A for the Durham scaling law whereas the ITER scaling law gives ~ 3.3 A. The parameterisation covers the field range from 6.5 T to 14.5 T and the temperature range from 4.2 K to 12 K. In total 559 $J_C(B,T,\varepsilon)$ data points have been fitted.

The values of r and s derived from the n-value data for the OST strand were 2.83 and 0.45 respectively.

p	q	$\boldsymbol{n}$	$\boldsymbol{\nu}$	$\boldsymbol{w}$	$\boldsymbol{u}$	ε_M (%)
0.963	2.310	***2.500***	***1.500***	***2.200***	***0***	0.254

$A(0)$ ($Am^{-2}T^{3-n}K^{-2}$)	$T_C^*(0)$ (K)	$B_{C2}^*(0,0)$ (T)	c_2	c_3	c_4
4.283×10^7	16.73	30.76	–0.753	–0.606	–0.160

Table II: Durham scaling law parameters for the OST internal-tin strand derived from variable strain, field and temperature data using 9 free-parameters. Data were obtained at 4.2, 8, 10 and 12 K. The four parameters in bold were not varied in the fitting procedure. (RMS ~ 2.8 A)

p	q	C (ATm^{-2})	C_{a1}	C_{a2}
0.746	2.335	5.421×10^{10}	79.94	45.04

$\varepsilon_{0,a}$ (%)	ε_M (%)	$B_{C20max}^*(0,0)$ (T)	$T_{C0max}^*(0)$ (K)
0.207	0.284	32.59	16.26

Table III: The official ITER scaling parameters for the OST strand derived from variable field, variable temperature and variable strain data – 9 free parameters. Data fitting was limited to 4.2, 8, 10 and 12 K. (RMS ~ 3.3 A)

3.3.4 Parameterisation of the BEASI and BEASII strands.

The $J_C(B,T,\varepsilon)$ data of BEASI and BEASII strands were parameterized using the Durham Scaling law with 9 free-parameters. The parameters from the Durham Scaling law are given in tables IV and VI and the official 9 free-parameter ITER fit is shown in tables V and VII. These scaling results are plotted graphically in figures 8-11 as solid and dotted lines For the BEASI strand the parameterisation covers the field range from 7.5 T to 14.5 T, and the temperature range from 4.2 K to 10 K. In total 306 $J_C(B,T,\varepsilon)$ data points have been fitted. While for the BEASII strand the parameterisation covers the field range from 6.5 T to 14.5 T and the temperature range from 4.2 K to 12 K. In total 489 $J_C(B,T,\varepsilon)$ data points have been fitted.

The values of r and s derived from the n-value data for the BEASI strand were 2.97 and 0.50 respectively and equivalent values for the BEASII strand were 3.03 and 0.50.

p	q	$\boldsymbol{n}$	$\boldsymbol{\nu}$	$\boldsymbol{w}$	$\boldsymbol{u}$	ε_M (%)
1.056	2.099	***2.500***	***1.500***	***2.200***	***0***	0.382

$A(0)$ ($Am^{-2}T^{3-n}K^{-2}$)	$T_C^*(0)$ (K)	$B_{C2}^*(0,0)$ (T)	c_2	c_3	c_4
3.317×10^7	16.60	29.80	-0.487	-0.263	-0.0420

Table IV: Durham scaling law parameters for BEASI strand derived from variable strain, field and temperature data using 9 free-parameters. Data were obtained at 4.2 and 10 K. The four parameters in bold were not varied in the fitting procedure (RMS ~ 3.2 A).

p	q	C (ATm^{-2})	C_{a1}	C_{a2}
0.525	1.547	2.357×10^{10}	404.87	386.71

$\varepsilon_{0,a}$ (%)	ε_M (%)	$B_{C20max}^*(0,0)$ (T)	$T_{C0max}^*(0)$ (K)
0.139	0.422	29.88	16.06

Table V: The official ITER scaling parameters for BEASI strand derived from variable field, variable temperature and variable strain data – 9 free parameters. Data were obtained at 4.2 and 10 K. (RMS ~ 3.8 A).

p	q	$\boldsymbol{n}$	$\boldsymbol{\nu}$	$\boldsymbol{w}$	$\boldsymbol{u}$	ε_M (%)
0.490	1.420	***2.500***	***1.500***	***2.200***	***0***	0.369

$A(0)$ ($Am^{-2}T^{3-n}K^{-2}$)	$T_C^*(0)$ (K)	$B_{C2}^*(0,0)$ (T)	c_2	c_3	c_4
1.434×10^7	16.36	28.75	-0.435	-0.219	-0.0325

Table VI: Durham scaling law parameters for BEASII strand derived from variable strain, field and temperature data using 9 free-parameters. Data were obtained at 4.2, 8, 10 and 12 K. The four parameters in bold were not varied in the fitting procedure. (RMS ~ 2.4 A).

p	q	C (ATm^{-2})	C_{a1}	C_{a2}
0.489	1.618	2.227×10^{10}	226.93	203.86
$\varepsilon_{0,a}$ (%)	ε_M (%)	$B_{C20max}^*(0,0)$ (T)		$T_{C0max}^*(0)$ (K)
0.187	0.366	30.28		16.02

Table VII: The official ITER scaling parameters for BEASII strand derived from variable field, variable temperature and variable strain data – 9 free parameters. Data were obtained at 4.2, 8, 10 and 12 K. (RMS ~ 2.5 A).

4 CORRELATION: HIGHER CRITICAL CURRENT DENSITY – HIGHER STRAIN SENSITIVITY.

Figure 16 shows both the absolute values and the normalised values of the critical current density as function of strain at 12 T and 14 T. Consistent with the clear trends in the parameterisation values of the Durham scaling law fits (cf Tables II, IV and VI), higher J_C is associated with higher intrinsic parameters $T_C^*(0)$ and $B_{C2}^*(0,0)$ and higher $|c_2|$ and $|c_3|$. This leads to greater strain sensitivity for the current density in higher J_C samples.

Figures 17 and 18 show a clear pivot point in compressive strain which increases with increasing field and temperature. Changing the strain from one side of the pivot point side to the other changes the highest J_C sample to the lowest J_C sample and vice versa. For the three samples measured, at 4.2K and 12 T the pivot point has a compressive strain value of -0.9 % that increases to -0.7% at 14 T as shown in Fig. 19.

The relationship between the *n*-value and critical current (I_C) has been parameterised using a modified power law of the form $n = 1+rI_C^s$, where *r* and *s* are constants. The OST sample has the lowest *n*-values. The *n*-values (and values of *r* and *s*) are similar for the two BEAS strands. As

shown in Fig. 20, the normalized *n*-values of the different types of Nb_3Sn strand show quite similar strain behaviour as a function of intrinsic strain.

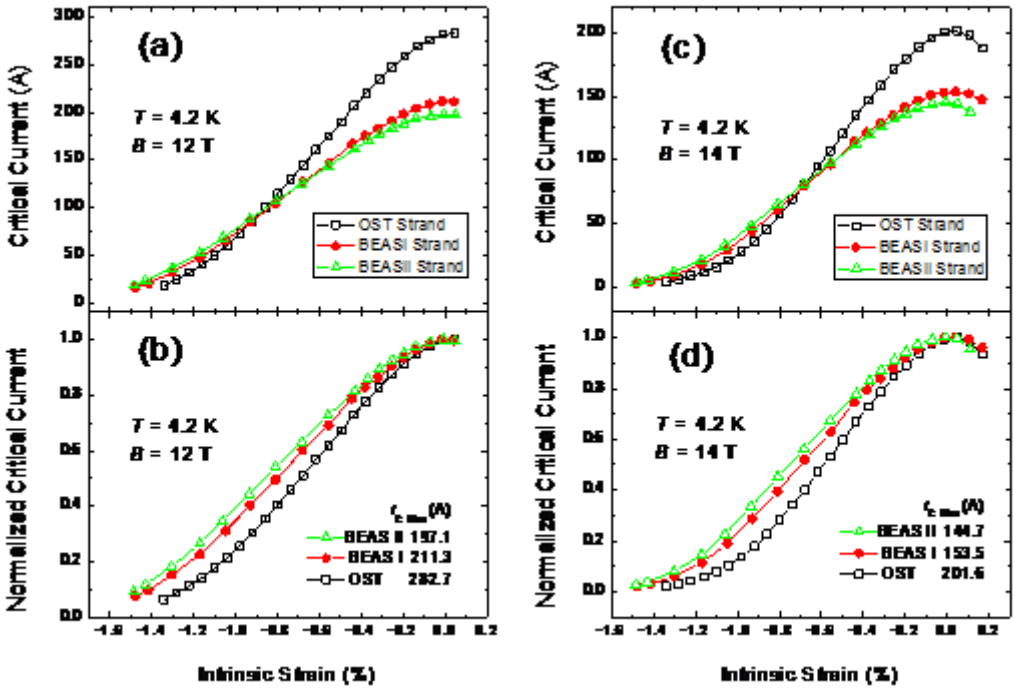

Fig. 16: Critical current and normalized critical current as functions of intrinsic strain at T = 4.2 K and at magnetic fields equal 12 and 14 T for the three strands measured in this report. The lines are guides to the eye.

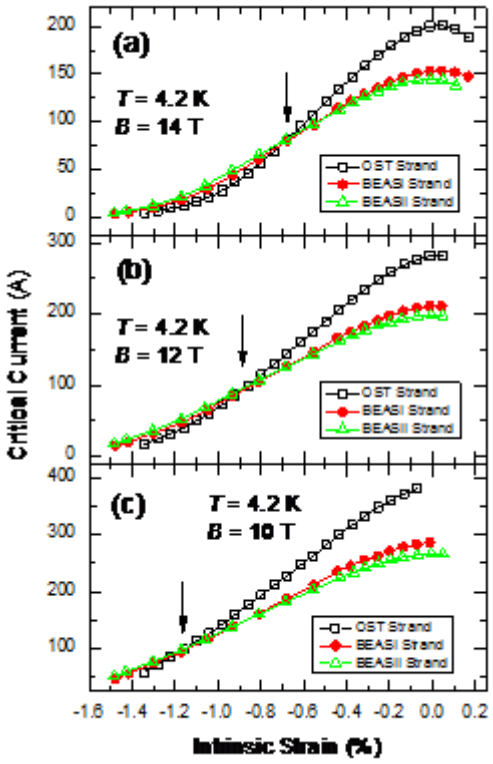

Figure 17: Critical current (I_C) as a function of intrinsic strain at 4.2 K and at (a) 14 T, (b) 12 T and (c) 10 T for all three stands measured. Note that at a fixed magnetic field I_C of all samples coincide on one intrinsic strain (indicated by arrows in the figure).

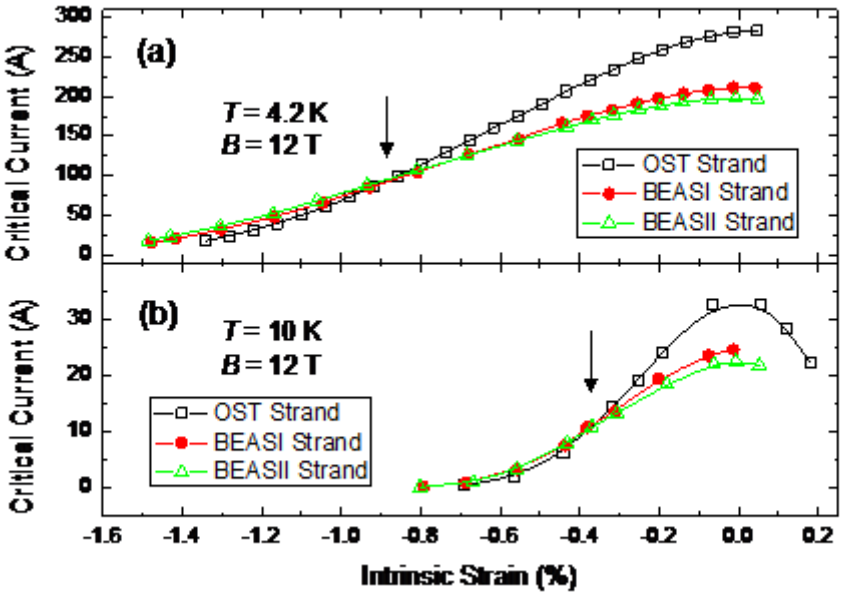

Figure 18: Intrinsic strain dependence of critical current (I_C) at 12 T and at (a) 4.2 K and (b) 10 K for all three strands measured. At a fixed temperature I_C of all strands meet at one intrinsic strain as indicated by arrows in the figure.

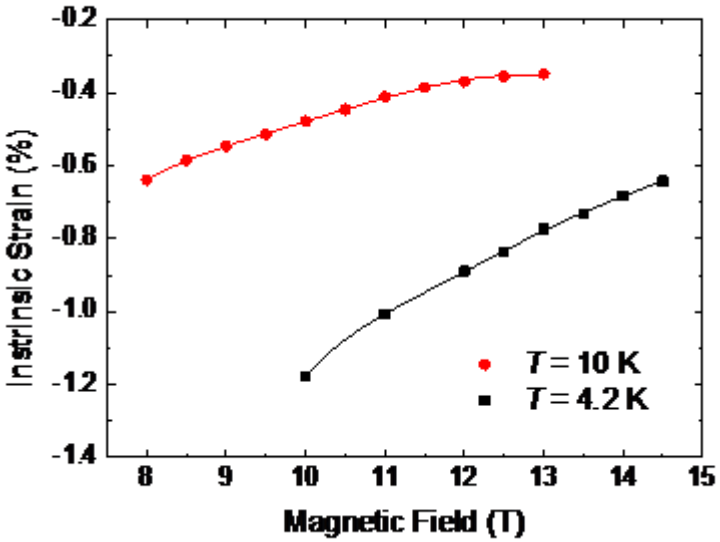

Figure 19: Pivot points of the strands at 4.2 K and 10 K. The lines are guides to the eye.

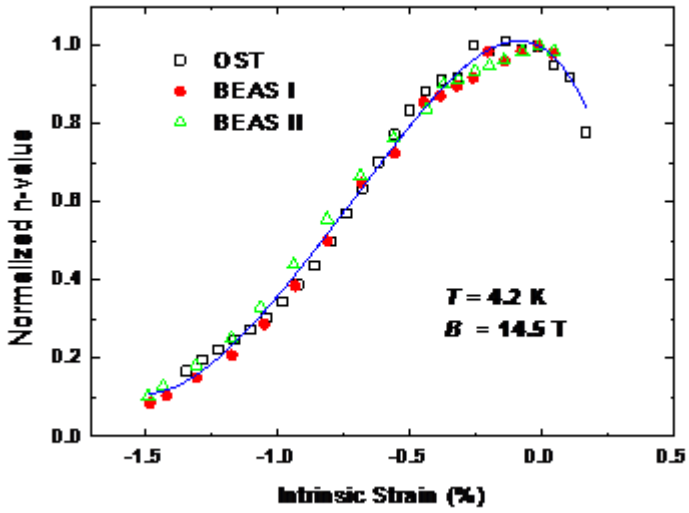

Fig. 20: Normalized *n*-values as a function of intrinsic strain for the three strands measured in this report. The line is guide to the eye.

5 CONCLUDING COMMENTS.

We have reported the engineering critical current density ($J_C(B,T,\varepsilon)$) at 10 μVm^{-1} and $n(B,T,\varepsilon)$ over the range 10 – 100 μVm^{-1} as a function of magnetic field, temperature and uniaxial strain for OST, BEASI and BEASII strands. The three strands are parameterised using the Durham scaling law and the ITER scaling law both of which have nine free-parameters – the RMS values show that the $J_C(B,T,\varepsilon)$ data is most accurately described using the Durham Scaling law.

The reversibility of the critical current data as a function of strain is excellent.

Comparisons with data produced in Durham, shows that reproducibility of the Durham variable strain data over many years is excellent.

Consistent with the clear trends in the parameterisation values of the Durham scaling law fits (cf Tables II, IV and VI), higher J_C is associated with higher intrinsic parameters $T_C^*(0)$ and $B_{C2}^*(0,0)$ and higher $|c_2|$ and $|c_3|$. This leads to greater strain sensitivity for the current density in higher J_C samples and pivot points.

The relationship between the *n*-value and critical current (I_C) has been parameterised for aqll thre strands using a modified power law of the form $n = 1+rI_C^s$, where *r* and *s* are constants. The OST sample has the lowest *n*-values.

Accompanying this report are three spreadsheets that contain tabulations of the J_C and *n*-value data, as well as the scaling-law parameterisation of $J_C(B,T,\varepsilon)$ for OST, BEASI and BEASII strands respectively at: http://www.dur.ac.uk/superconductivity.durham/publications.html

REFERENCES

1 D M J Taylor and D P Hampshire, "The scaling law for the strain dependence of the critical current density in Nb_3Sn superconducting wires," Supercond. Sci. Tech. **18**, S241-S252 (2005).

2 D M J Taylor and D P Hampshire, "Properties of helical springs used to measure the axial strain dependence of the critical current density in superconducting wires," Supercond. Sci. Tech. **18**, 356-368 (2005).

3 C R Walters, I M Davidson, and G E Tuck, "Long sample high sensitivity critical current measurements under strain," Cryogenics **26**, 406-412 (1986).

4 N Cheggour and D P Hampshire, "A probe for investigating the effects of temperature, strain, and magnetic field on transport critical currents in superconducting wires and tapes," Rev. Sci. Instrum. **71** (12), 4521-4530 (2000).

5 S A Keys, N Koizumi, and D P Hampshire, "The strain and temperature scaling law for the critical current density of a jelly-roll Nb_3Al strand in high magnetic fields," Supercond. Sci. Tech. **15**, 991-1010 (2002); S A Keys and D P Hampshire, in *Handbook of Superconducting Materials*, edited by D Cardwell and D Ginley (IOP Publishing, Bristol, 2003), Vol. 2, pp. 1297-1322.

6 X F Lu, D M J Taylor, and D P Hampshire, "Critical current scaling laws for advanced Nb_3Sn superconducting strands for fusion applications with six free parameters," Superconductor Science & Technology **21** (10), 105016 (2008).

7 L Bottura, "$J_C(B,T,\varepsilon)$ Parameterization for the ITER Nb_3Sn Production," EFDA Intermediate Report, 1-23 (2008).

8 B ten Haken, A Godeke, and H H J ten Kate, "The influence of compressive and tensile axial strain on the critical properties of Nb_3Sn conductors," IEEE Trans. Appl. Supercond. **5** (2), 1909-1912 (1995); W D Markiewicz, "Elastic stiffness model for the critical temperature T_C of Nb_3Sn including strain dependence," Cryogenics **44**, 767-782 (2004); W D Markiewicz, "Invariant formulation of the strain dependence of the critical temperature T_C of Nb_3Sn in a three term approximation," Cryogenics **44**, 895-908 (2004); W D Markiewicz, "Comparison of strain scaling functions for the strain dependence of composite Nb_3Sn superconductors," Superconductor Science & Technology **21**, 054004 (2008).

9 A Godeke, B ten Haken, H H J ten Kate et al., "A general scaling relation for the critical current density in Nb_3Sn," Superconductor Science & Technology **19**, R100-R116 (2006).

10 D P Hampshire, "Publication list and Excel files with the raw data on the group website," http://www.dur.ac.uk/superconductivity.durham/ (2008).

11 P Bruzzone, "The index *n* of the voltage–current curve, in the characterization and specification of technical superconductors," Physica C **401** (1-4), 7-14 (2004).

12 D P Hampshire and H Jones, "Critical current of a NbTi reference material as a function of field and temperature," Magnet Technology 9, 531-535 (1985).

13 D P Hampshire and H Jones, "Analysis of the general structure of the *E-I* characteristic of high current superconductors with particular reference to a NbTi SRM wire," Cryogenics **27**, 608-616 (1987).

14 W H Warnes and D C Larbalestier, "Critical current distributions in superconducting composites," Cryogenics **26**, 643-653 (1986).

15 A K Ghosh, "*V-I* transition and *n*-value of multifilamentary LTS and HTS wires and cables," Physica C **401** (1-4), 15-21 (2004).

16 J Baixeras and G Fournet, "Pertes par deplacement de vortex dans un supraconducteur de type II non ideal," J. Phys. Chem. Solids **28**, 1541-1547 (1967); H S Edelman and D C

Larbalestier, "Resistive transitions and the origin of the n value in superconductors with a gaussian critical-current distribution," J. Appl. Phys. **74** (5), 3312-3315 (1993).

[17] W H Warnes, "A model for the resistive critical current transition in composite superconductors," J. Appl. Phys. **63** (5), 1651-1662 (1988); W H Warnes and D C Larbalestier, "Analytical technique for deriving the distribution of critical currents in a superconducting wire," Appl. Phys. Lett. **48** (20), 1403-1405 (1986).

[18] R Wördenweber, "Mechanism of vortex motion in high-temperature superconductors," Rep. Prog. Phys. **62**, 187 -236 (1998).

[19] D M J Taylor, S A Keys, and D P Hampshire, "*E-J* characteristics and *n*-values of a niobium-tin superconducting wire as a function of magnetic field, temperature and strain," Physica C **372**, 1291-1294 (2002).